# Thermocapillary instability in a viscoelastic liquid layer under an imposed oblique temperature gradient

Cite as: Phys. Fluids **33**, 012107 (2021); https://doi.org/10.1063/5.0036202
Submitted: 03 November 2020 . Accepted: 21 December 2020 . Published Online: 22 January 2021

Ramkarn Patne, Yehuda Agnon, and Alexander Oron

# Thermocapillary instability in a viscoelastic liquid layer under an imposed oblique temperature gradient

Cite as: Phys. Fluids 33, 012107 (2021); doi: 10.1063/5.0036202
Submitted: 3 November 2020 • Accepted: 21 December 2020 •
Published Online: 22 January 2021



Ramkarn Patne,[1,2] Yehuda Agnon,[1] and Alexander Oron[2,a)]

## AFFILIATIONS

[1] Faculty of Civil and Environmental Engineering, Technion-Israel Institute of Technology, Haifa 3200003, Israel
[2] Faculty of Mechanical Engineering, Technion-Israel Institute of Technology, Haifa 3200003, Israel

[a)] Author to whom correspondence should be addressed: meroron@technion.ac.il

## ABSTRACT

The linear stability analysis of a viscoelastic (Oldroyd-B) liquid layer subjected to an oblique temperature gradient (OTG) is investigated numerically. For the case of low liquid elasticity, the analysis shows a strong stabilizing effect of the horizontal component (HTG) of the OTG on the two elastic modes emerging due to the presence of the vertical component (VTG) of the OTG. However, if the liquid elasticity is sufficiently large, the HTG fails to stabilize the upstream elastic mode. The liquid elasticity stabilizes the Newtonian interaction mode arising out of the interaction between the HTG and the VTG. The thermocapillary flow introduced by the HTG leads to the development of a new elastic mode absent in the case of a Newtonian liquid layer. The present paper thus shows that the elasticity of the liquid plays a major role in the competition between various instability modes to determine the dominant mode of instability.



## I. INTRODUCTION

Viscoelastic liquid layers subjected to an oblique temperature gradient (OTG) are found in numerous industrial processes and scientific experimental settings. In industrial processes such as additive manufacturing,[1] material processing and crystal growth,[2] coating and drying operations,[3] layers of viscoelastic fluids are frequently present in nonisothermal processes, which may lead to the emergence of a nonuniform temperature field in the bulk and along the free surface. Viscoelastic fluids are also abundant in microfluidics[4] and polymer patterning.[5,6]

Thermocapillary instability may arise because of the temperature dependence of the surface tension in a liquid layer and an ensuing emergence of tangential stresses at the layer interface exposed to the ambient gas phase. Thermocapillary or Marangoni instability in a layer of a Newtonian liquid subjected to a purely vertical (normal to the solid substrate) temperature gradient, the vertical component (VTG), was first studied theoretically by Pearson.[7] His study was inspired by the experimental observations of Bénard.[8] Pearson[7] showed the emergence of the Marangoni instability of a finite critical wavenumber in a layer with a nondeformable interface if the temperature was fixed at the substrate. He also showed that in the case of a fixed temperature gradient at the substrate, the instability may be long-wave. The investigation of the Marangoni instability was further extended[9–12] to liquid layers with a deformable interface and revealed a strong effect of deformability expressed by a finite capillary number.

Another class of thermocapillary instabilities emerges when a layer of a Newtonian fluid is subjected to an imposed purely horizontal (tangential to the substrate) temperature gradient, the horizontal component (HTG), that affects the onset and the character of the emerging instability.[13] This setting was first investigated by Smith and Davis[14,15] who showed the emergence of oblique hydrothermal waves and spanwise rolls as a result of the thermocapillary instability in this configuration where the base state is not quiescent as in the layer subjected to a VTG but represents a flow driven by the Marangoni stresses in the direction opposite to that of the imposed HTG. The instabilities predicted in their study have been observed in experiments.[16–21]

Thermocapillary instabilities in a viscoelastic liquid layer subjected to a purely VTG was first studied by Getachew and Rosenblat[22] in the case of a nondeformable interface and then by

several other authors[23–26] for Maxwell and Jeffreys liquids. Recently, Patne *et al.*[27] studied the Marangoni instability in a layer of a linear Jeffreys liquid layer with a deformable interface. Their analyses revealed the emergence of both stationary and oscillatory modes of instability. As in the case of a Newtonian fluid layer, deformability of the layer interface promotes long-wave instability for larger capillary numbers and short-wave instability for small capillary numbers. Here, the terms stationary and oscillatory instabilities refer to the cases when the leading eigenvalue of the spectrum of the corresponding problem has a zero real part with a zero or nonzero imaginary part, respectively. The stationary instability mode is due to the viscous component of the stresses since it is excited in a layer of a Newtonian fluid. However, the elastic part of the fluid stresses gives rise to two symmetric modes possessing an equal growth rate but a phase speed of differing signs corresponding to the propagation in the opposite directions. A coupled Rayleigh (buoyancy-driven)–Marangoni convection in thin polymeric layers was experimentally studied, and hexagonal patterns were observed.[28]

The work of Smith and Davis[14] was extended to non-Newtonian fluids and droplets by Hu and co-workers.[29–31] Hu *et al.*[29] studied an Oldroyd-B liquid layer subjected to a purely HTG. They found the existence of three classes of unstable modes, viz., oblique wave, streamwise wave, and spanwise stationary modes. All the three modes were found to be significantly affected by the variation in the elasticity of the liquid. The spanwise stationary mode was shown to be the dominant mode of instability for highly elastic liquid. As shown in Sec. IV, for a highly elastic liquid layer subjected to an OTG, it is the elastic mode introduced by the VTG that dominates the instability, which holds true even when the strength of the imposed VTG is negligibly smaller than the imposed HTG. This shows that a mere presence of the VTG component can drastically alter the stability picture, thereby illustrating the need to study the present problem.

It needs to be realized that in experiments dealing with thermocapillarity, application of a purely vertical or horizontal temperature gradient may be difficult, and then inadvertently, a liquid layer becomes subjected to an oblique temperature gradient (OTG) with the HTG and VTG. Due to such a presence of imperfection related to the orientation of the temperature gradient with respect to the layer itself, several authors undertook studies[1,32–38] of the thermocapillary instabilities in a Newtonian-liquid layer under an OTG. Their analyses demonstrated a strong stabilizing effect of the imposed HTG component on the instabilities caused by the imposed VTG. The experiments of Schwabe[21] and Mizev and Schwabe[39] confirmed these theoretical results.

These considerations motivated the present study for a non-isothermal viscoelastic liquid layer subjected to an OTG with an emphasis on the thermocapillary instability. To account for the viscoelasticity of the fluid, we employ a quasilinear Oldroyd-B model due to its relative "simplicity," which is yet capable of qualitatively representing the dynamic features of a viscoelastic liquid. The present investigation aims to understand the effect of the HTG on the thermocapillary instabilities introduced by the imposed VTG and vice versa. Thus, the results obtained here may provide guidelines for future experimental studies carried out to understand the emergence of the thermocapillary instabilities in a viscoelastic liquid layer subjected to an OTG.

The rest of the paper is arranged as follows: The problem statement, the original governing equations, and the boundary conditions, the base-state fields, and the governing equations for the perturbations are all brought out in Sec. II. The pseudospectral numerical approach used in the solution of the linear eigenvalue problem for the linear stability analysis is briefly outlined in Sec. III. The results of the linear stability analysis of the base-state flow and the related discussion are presented in Sec. IV. The major conclusions of the present paper are summarized in Sec. V.

## II. PROBLEM FORMULATION

We consider a three-dimensional layer of an incompressible viscoelastic liquid of a mean thickness $d$ deposited on the upper surface of a horizontal planar solid substrate in the gravity field $g$. The physical properties of the fluid such as density $\rho$, thermal conductivity $k_{th}$, thermal diffusivity $\kappa$, and the relaxation and retardation constants $\lambda_1$ and $\lambda_2$, respectively, are assumed to be temperature-independent. The viscosity $\mu_0$ is also assumed to be temperature-independent. Note that the subscript 0 denotes the zero-shear viscosity, which is the viscosity of a polymer solution before shear-thinning sets in. The latter is observed in the case of concentrated polymer solutions and polymer melts.[40] Since the Oldroyd-B model does not exhibit shear-thinning, it is applicable in a zero-shear domain. For dilute polymer solutions, viscosity is a weak function of the shear-rate.[41] Hence, the Oldroyd-B model is valid for an arbitrary shear-rate. We also denote this by $\nu = \mu_0/\rho$, the kinematic viscosity of the fluid. The layer is assumed to be sufficiently thin, so the buoyancy effect could be neglected.

The layer is assumed to be of an infinite lateral extent and bounded by the ambient inert gas phase at the upper surface, which is assumed to be deformable. The coordinate system used here is Cartesian with the axes $x^*$ and $z^*$ located within the substrate plane, whereas the axis $y^*$ is normal to the substrate and directed into the liquid layer with the reference point $y^* = 0$ located on the substrate plane. In what follows, the asterisk denotes dimensional variables, whereas their dimensionless counterparts are denoted without an asterisk.

The temperature of the planar substrate is imposed to vary linearly in the $x^*$-direction as $T_0^* - \eta^* x^*$, whereas that of the ambient gas phase is $T_\infty^* - \eta^* x^*$ so the temperature difference across the layer $\Delta T^* \equiv T_0^* - T_\infty^* > 0$, where $T_0^*$ and $T_\infty^*$ are constant reference temperatures and $\eta^*$ is the imposed HTG. Thus, the entire system containing the substrate, the liquid layer, and the gas phase is subjected to a constant HTG in the $x^*$-direction.

The present setting suggests that the temperature field in the liquid layer varies in both vertical and horizontal directions, hence depending on both $x^*$ and $y^*$; thus, an OTG is imposed on the layer. We note in passing that, as shown below in Eq. (9b), the base-state temperature has a cubic term in addition to the linear term varying in the vertical direction $y$. The cubic term in $y$ arises due to the presence of advection of energy.

Surface tension at the liquid–gas interface $\sigma*$ is assumed to be temperature-dependent,

$$\sigma^* = \sigma_0^* - \sigma_T^*(T^* - T_0^*), \tag{1}$$

where $\sigma_T^* \equiv -\frac{d\sigma^*}{dT^*} > 0$ and $\sigma_0^*$ is the reference surface tension of the fluid at the reference temperature of the lower plate taken as $T_0^*$.

To nondimensionalize the governing equations of the problem, length, time, velocity, and temperature are normalized with respect to $d$, $d^2/\kappa$, $\kappa/d$, and $a^* d$, respectively, where $a^*$ is the imposed vertical temperature gradient (VTG) to be specified below. Furthermore, pressure and stresses are nondimensionalized by $\mu_0\kappa/d^2$.

We denote the dimensionless fluid velocity, pressure, and temperature fields by $\mathbf{v} = (v_x, v_y, v_z)$, with $v_i$ being the velocity components in the direction $i = x, y, z$; $p$ and $T$, respectively, and $\boldsymbol{\tau}$ is the stress tensor. The dimensionless continuity and momentum conservation (Cauchy) equations are

$$\nabla \cdot \mathbf{v} = 0, \tag{2a}$$

$$\frac{1}{Pr}[\partial_t \mathbf{v} + (\mathbf{v}\cdot\nabla)\mathbf{v}] = -\nabla p - GPr\nabla y + \nabla\cdot\boldsymbol{\tau}, \tag{2b}$$

where $Pr = \mu_0/\rho\kappa$ is the Prandtl number, $G = gd^3/\nu^2$ is the Galileo number, $\nabla = (\partial_x, \partial_y, \partial_z)$ is the gradient operator, $\nabla^2 \equiv \partial_x^2 + \partial_y^2 + \partial_z^2$ is the Laplacian operator, $p$ is the pressure, and $\partial_i$ denotes the partial derivative with respect to the variable $i$. The dimensionless heat advection-diffusion equation is

$$\partial_t T + (\mathbf{v}\cdot\nabla)\, T = \nabla^2 T. \tag{2c}$$

The governing equations (2) are subjected to the following boundary conditions: no-slip, impermeability, and a specified temperature at the solid substrate $y = 0$ yields

$$v_x = 0, \quad v_y = 0, \quad v_z = 0, \quad T = T_0 - \eta x, \tag{3a}$$

where $\eta = \eta^*/a^*$ represents the dimensionless HTG.

At the deformable gas–liquid interface located at $y = 1 + \xi(x, y, t)$, $\xi(x, z, t)$ representing the infinitesimal displacement of the interface from its undisturbed position $y = 1$. The boundary conditions at the interface represent the kinematic boundary condition, the tangential and normal components of the stress balance,[12] and the continuity of the heat flux, respectively, is

$$\partial_t \xi + \mathbf{v}_\perp \cdot \nabla\xi = v_y, \tag{3b}$$

$$\mathbf{t}_j \cdot \boldsymbol{\tau} \cdot \mathbf{n} = -Ma\nabla T \cdot \mathbf{t}_j, \tag{3c}$$

$$-p + \mathbf{n}\cdot\boldsymbol{\tau}\cdot\mathbf{n} = -Ca^{-1}(\nabla\cdot\mathbf{n}) - Bo\, Ca^{-1}\xi, \tag{3d}$$

$$\nabla T \cdot \mathbf{n} = -Bi(T - T_\infty + \eta x), \tag{3e}$$

where

$$Ma = \frac{\gamma^* a^* d^2}{\mu_0\kappa}, Bo = \frac{\rho g d^2}{\sigma_0^*}, Bi = \frac{qd}{k_{th}}, Ca = \frac{\mu_0\kappa}{\sigma_0^* d} \tag{4}$$

are, the Marangoni, Bond, Biot and capillary numbers, respectively, $Bo = GCa$ and $j = 1, 2$. Here $q$, $\sigma_0^*$, $g$, and $k_{th}$ are the coefficient of thermal convection at the free surface, surface tension evaluated at the free surface temperature, gravity acceleration, and thermal conductivity of the fluid, respectively. The vectors $\mathbf{t}_j$ and $\mathbf{n}$ represent the unit tangent and normal vectors to the free surface, respectively. In addition, the vector $\mathbf{v}_\perp$ is a two-dimensional vector obtained by projection of $\mathbf{v}$ onto the $x$–$z$ plane, $\mathbf{v}_\perp = (v_x, v_z)$. The linearized expressions, i.e., not containing the interfacial metrics, for the normal $\mathbf{n}$ and tangential vectors $\mathbf{t_1}$ and $\mathbf{t_2}$ at the free surface in the perturbed state are

$$\mathbf{n} = -\partial_x\xi\,\mathbf{e_x} + \mathbf{e_y} - \partial_z\xi\,\mathbf{e_z}, \quad \mathbf{t}_1 = \mathbf{e_x} + \partial_x\xi\,\mathbf{e_y}, \quad \mathbf{t}_2 = \partial_z\xi\,\mathbf{e_y} + \mathbf{e_z}. \tag{5}$$

The vectors $\mathbf{e_x}$, $\mathbf{e_y}$, and $\mathbf{e_z}$ are the unit vectors in $x$, $y$, and $z$-directions, respectively.

In what follows, we use the Oldroyd-B model[42] to describe the relationship between the shear stress $\boldsymbol{\tau}$ and the strain rate $\dot{\boldsymbol{\gamma}}$ in the viscoelastic fluid, which reads

$$\boldsymbol{\tau} + W\left(\frac{\partial\boldsymbol{\tau}}{\partial t} + (\mathbf{v}\cdot\nabla)\boldsymbol{\tau} - (\nabla\mathbf{v})^T\cdot\boldsymbol{\tau} - \boldsymbol{\tau}\cdot(\nabla\mathbf{v})\right) = \dot{\boldsymbol{\gamma}} + \beta\left(\frac{\partial\dot{\boldsymbol{\gamma}}}{\partial t} + (\mathbf{v}\cdot\nabla)\dot{\boldsymbol{\gamma}} - (\nabla\mathbf{v})^T\cdot\dot{\boldsymbol{\gamma}} - \dot{\boldsymbol{\gamma}}\cdot(\nabla\mathbf{v})\right), \tag{6a}$$

$$\dot{\boldsymbol{\gamma}} = (\nabla\mathbf{v}) + (\nabla\mathbf{v})^T, \tag{6b}$$

where

$$W = \frac{\lambda_1\kappa}{d^2}, \quad \beta = \frac{\lambda_2\kappa}{d^2} \tag{7}$$

are the Weissenberg number and dimensionless retardation time, respectively. For vanishing $\lambda_1$ and $\lambda_2$, the Oldroyd-B model reduces to a Newtonian fluid model. It must be also noted that the Oldroyd-B model represents an extension of the linear Jeffreys fluid model to include the effect of the base-state flow present in the system under consideration. Thus, if the imposed HTG is turned off, i.e., $\eta = 0$, then the Oldroyd-B model reduces to the Jeffreys model, and the results regarding the stability of the thermocapillary flow in the system will reduce to those for the viscoelastic liquid layer subjected to a pure VTG,[23,27] whereas in the case of $\lambda_1 = 0$ and $\lambda_2 = 0$, the results will reduce to those for a Newtonian liquid layer with a deformable interface subjected to an oblique temperature gradient considered by Patne *et al.*[37]

The Oldroyd-B model is applicable for dilute polymer solutions, which do not exhibit a strong shear-thinning, whereas for concentrated polymer solutions and polymer melt non-linear models, FENE-P, Giesekus, and White-Metzner models,[41,43] reptation based pom-pom[44] and Rolie-Poly[45] models are appropriate. The Oldroyd-B model used here can faithfully describe polymer flows for a low-shear rate such that the fluid exhibits shear-thinning in which case its viscosity is referred to as the zero-shear viscosity. The results discussed here are thus restricted to either dilute polymer solutions with a negligible shear-thinning or to a low shear-rate domain in the case of concentrated polymer solutions and polymer melts.

### A. Base state

For the base state, the governing equations (2) are amended with the boundary conditions expressing no-slip, impermeability, and a constant temperature gradient at the solid substrate $y = 0$,

$$\bar{v}_x = 0, \quad \bar{v}_y = 0, \quad \bar{v}_z = 0, \quad \bar{T} = T_0 - \eta x. \tag{8a}$$

At the undisturbed gas–liquid interface $y = 1$, the boundary conditions are the kinematic boundary condition, the tangential component of the stress balance, and the continuity of the heat

flux, respectively,

$$\bar{v}_y = 0, \quad \bar{\tau}_{xy} = -Ma\partial_x \bar{T}, \quad \partial_y \bar{T} = -Bi(\bar{T} - T_\infty + \eta x), \tag{8b}$$

The governing equations (2) and the boundary condition equations (8) determine the base state in the form

$$\bar{v}_x = \eta\, Ma\, y, \quad \bar{v}_y = 0, \quad \bar{v}_z = 0, \quad \bar{p} = p_a - G\,Pr\, y, \tag{9a}$$

$$\bar{T}(x,y) = T_0 - \eta x + \left[\frac{\eta^2 Ma}{2(1+Bi)}\left(1+\frac{Bi}{3}\right) - 1\right]y - \frac{\eta^2 Ma}{6}y^3. \tag{9b}$$

Note also that the vertical component of the temperature gradient $a^*$ is related to the temperature drop across the layer $\Delta T^*$ via

$$a^* = \frac{Bi\Delta T^*}{(1+Bi)d}. \tag{10}$$

It follows from Eq. (9b) that, similar to the case considered by Patne *et al.*,[37] in addition to the vertical component of the imposed OTG, the HTG *induces* an additional VTG, which has a positive sign and counteracts the imposed negative VTG. Furthermore, the induced VTG is proportional to $\eta^2$ and is always positive for positive Marangoni numbers. As shown in Sec. IV, the induced VTG has a strong effect on the Marangoni instability set by the imposed VTG.

The base-state stresses in the liquid layer are obtained from Eq. (6a),

$$\bar{\tau}_{xx} = 2(W-\beta)\left(\frac{d\bar{v}_x}{dy}\right)^2, \quad \bar{\tau}_{xy} = \frac{d\bar{v}_x}{dy}, \quad \bar{\tau}_{yy} = 0 \tag{11}$$

with the rest of the stresses $\tau_{zi} = 0$ for all $i$. For physically relevant viscoelastic liquids, $W > \beta$, so the first normal stress difference, i.e., $\tau_{xx} - \tau_{yy}$, is positive, as dictated by the rules of the rheological analysis.[41]

### B. Perturbed state

Next, infinitesimally small perturbations are imposed on the base state equation (9) to carry out the linear stability analysis of the system. Although Squire's theorem[46] is not applicable in the present case due to the imposed HTG, Patne *et al.*[37] demonstrated that two-dimensional disturbances are more unstable than the corresponding three-dimensional disturbances for a Newtonian liquid layer subjected to an oblique temperature gradient. In the same spirit, for the present problem, we assume two-dimensional disturbances.

The governing equations are then linearized around the base state equation (9) and normal modes

$$f'(\mathbf{x},t) = \tilde{f}(y)\exp(ikx+st), \quad \xi(x,t) = \tilde{\xi}\exp(ikx+st). \tag{12}$$

are substituted into those. Here, $f'(\mathbf{x},t)$ is a perturbation to a dynamic variable $f(\mathbf{x},t)$, such as the components of the fluid velocity field $v_x, v_y$, and $v_z$, pressure $p$, temperature $T$, and the components of the stress tensor $\boldsymbol{\tau}$, $\tilde{f}(y)$ is the corresponding complex eigenfunction in the Laplace–Fourier space, and $\tilde{\xi}$ is a constant. The parameter $k$ is the wavenumber of the perturbations in the $x$-direction, and the value $s = s_r + is_i$ is the complex growth rate. The base-state flow is linearly unstable if at least one eigenvalue satisfies the condition $s_r > 0$.

As a result of this procedure, the linearized continuity, momentum conservation, and energy equations become

$$ik\tilde{v}_x + D\tilde{v}_y = 0, \tag{13a}$$

$$\frac{1}{Pr}\left[s\tilde{v}_x + ik\bar{v}_x\tilde{v}_x + \tilde{v}_y D\bar{v}_x\right] = -ik\tilde{p} + ik\tilde{\tau}_{xx} + D\tilde{\tau}_{xy}, \tag{13b}$$

$$\frac{1}{Pr}\left[s\tilde{v}_y + ik\bar{v}_x\tilde{v}_y\right] = -D\tilde{p} + ik\tilde{\tau}_{xy} + D\tilde{\tau}_{yy}, \tag{13c}$$

$$s\tilde{T} + ik\bar{v}_x\tilde{T} + \partial_x\bar{T}\,\tilde{v}_x + \partial_y\bar{T}\,\tilde{v}_y = (D^2 - k^2)\tilde{T}, \tag{13d}$$

while the linearized constitutive equations become

$$\begin{aligned} &W\left[(ik\bar{v}_x + s)\tilde{\tau}_{xx} + \tilde{v}_y D\bar{\tau}_{xx} - 2ik\bar{\tau}_{xx}\tilde{v}_x - 2D\bar{v}_x\tilde{\tau}_{xy} - 2\bar{\tau}_{xy}D\tilde{v}_x\right] \\ &\quad + \tilde{\tau}_{xx} - 2ik\tilde{v}_x - 2i\beta ks\tilde{v}_x + 2\beta k^2\bar{v}_x\tilde{v}_x + 2i\beta kD\bar{v}_x\tilde{v}_y \\ &\quad + 4\beta D\bar{v}_x D\tilde{v}_x = 0, \end{aligned} \tag{13e}$$

$$\begin{aligned} &W\left[(ik\bar{v}_x + s)\tilde{\tau}_{xy} + \tilde{v}_y D\bar{\tau}_{xy} - ik\bar{\tau}_{xy}\tilde{v}_x - D\bar{v}_x\tilde{\tau}_{yy} - ik\bar{\tau}_{xx}\tilde{v}_y - \bar{\tau}_{xy}D\tilde{v}_y\right] \\ &\quad + \tilde{\tau}_{xy} - ik(1+\beta s)\tilde{v}_y - i\beta ks\tilde{v}_y + \beta k^2\bar{v}_x\tilde{v}_y + i\beta kD\bar{v}_x\tilde{v}_y \\ &\quad - (1+\beta s)D\tilde{v}_x - i\beta k\bar{v}_x D\tilde{v}_x + 3\beta D\bar{v}_x D\tilde{v}_y - \beta D^2\bar{v}_x\tilde{v}_y = 0, \end{aligned} \tag{13f}$$

and

$$\begin{aligned} &W\left[(ik\bar{v}_x + s)\tilde{\tau}_{yy} - 2ik\bar{\tau}_{xy}\tilde{v}_y\right] + \tilde{\tau}_{yy} + 2i\beta k\tilde{v}_y D\bar{v}_x - 2D\tilde{v}_y \\ &\quad - 2\beta sD\tilde{v}_y - 2i\beta k\bar{v}_x D\tilde{v}_y = 0, \end{aligned} \tag{13g}$$

where $D \equiv \frac{d}{dy}$. It must be noted that the linearized perturbation equation (13) is applicable for a general flow of a layer of an Oldroyd-B fluid possessing the base-state velocity field in the $x$-direction.

Equation (13) is next supplemented with the following boundary conditions: at $y = 0$, the no-slip and impermeability conditions at the lower plate imply

$$\tilde{v}_x = 0, \quad \tilde{v}_y = 0, \quad \tilde{T} = 0 \tag{14a}$$

at the deformable layer interface, and additional stresses are generated due to the presence of the Marangoni forces, which are responsible for the thermocapillary instabilities and base-state flow.

Thus, a standard procedure of projection of the boundary conditions specified at the deformed interface $y = 1 + \xi$ onto $y = 1$ leads to the boundary conditions at $y = 1$ in the form

$$\tilde{v}_y = s\tilde{\xi} + ik\bar{v}_x\tilde{\xi}, \tag{14b}$$

$$\tilde{\tau}_{xy} = -i\,k\,Ma\left(\tilde{T} + \partial_y\bar{T}\,\tilde{\xi}\right), \tag{14c}$$

$$-\tilde{p} + \tilde{\tau}_{yy} - 2ikD\bar{v}_x\tilde{\xi} = -\frac{(Bo + k^2)}{Ca}\tilde{\xi}, \tag{14d}$$

$$D\tilde{T} + Bi\tilde{T} + \left(-ik\partial_x\bar{T} + \partial_y^2\bar{T} + Bi\partial_y\bar{T}\right)\tilde{\xi} = 0. \tag{14e}$$

In the process of derivation of the normal stress balance boundary condition (14d), it has been assumed that the thermocapillary

contribution to the normal stress balance is negligible, i.e.,

$$\gamma^*\left(\tilde{T}^*|_{y^*=d} - T_0^*\right)/\sigma_0^* = Ma\ Ca\left(\tilde{T}|_{y=1} - T_0\right) \ll 1. \quad (15)$$

Since for most of the liquids $MaCa \ll 1$, this assumption is well justified provided that the temperature difference across the layer is not large. This also helps in proceeding with the normal mode analysis by removing the term $\tilde{T}|_{y=1}$, which explicitly depends on $x$ and therefore could have presented a technical obstacle.

Equations (13) and (14) constitute a generalized linear eigenvalue problem, which is to be solved for the eigenvalue $s$ and the eigenfunctions for a specified set of the parameter values $k, Bi, Bo, Ca, Pr,\ W, \beta$, and $Ma$. To determine the spectrum of the eigenvalue problem (13) and (14), the pseudospectral method is employed, and its details are in brief presented below.

## III. NUMERICAL APPROACH

To carry out the linear stability analysis of the problem at hand, the pseudospectral method is employed in which the eigenfunctions corresponding to each dynamic field are expanded into a series of the Chebyshev polynomials as

$$\widetilde{f}(y) = \sum_{m=0}^{m=N} a_{f,m} T_m(y), \quad (16)$$

where $T_m(y)$ are Chebyshev polynomials of degree $m$, $N$ is the highest degree of the polynomial in the series or, equivalently, the number of collocation points, and the coefficients of the series for all of the relevant dynamic fields such as $a_{f,m}$ in Eq. (16) are unknowns to be determined.

As a result of substitution of the expansions (16) into Eqs. (13) and (14), the problem is amenable to the generalized eigenvalue problem in the form

$$\mathbf{Ae} + s\mathbf{Be} = 0, \quad (17)$$

where $\mathbf{A}$ and $\mathbf{B}$ are matrices obtained from the discretization procedure and $\mathbf{e}$ is the vector containing the coefficients of all series expansions.

Further details of the discretization of the governing equations, boundary conditions, and construction of the matrices $\mathbf{A}$ and $\mathbf{B}$ can be found in the standard procedure described by Trefethen[47] and Schmid and Henningson.[46] Application of the pseudospectral method for similar problems was also described by Patne *et al.*[27,37] The MATLAB routine *polyeig* is used to solve the generalized eigenvalue problem given by Eq. (17). To filter out the spurious modes from the genuine numerically computed spectrum of the problem, the latter is determined from the solution with $N$ and $N+2$ collocation points, and the obtained eigenvalues are compared with a specified tolerance, e.g., $10^{-4}$. The genuine eigenvalues are verified by increasing the number of collocation points by 25 and monitoring their variation. Whenever the eigenvalue does not change up to a prescribed precision, e.g., to the sixth significant digit, the same number of collocation points is employed to determine the critical parameters of the system. In the present work, $N = 75$ was found to be sufficient to achieve the convergence and to determine the leading, most unstable eigenvalue for each parameter set within the investigated parameter range.

## IV. RESULTS AND DISCUSSION

In what follows, to investigate the instability of the system at hand, we consider polymer solutions whose physical properties belong to the range[19,28] $d \sim 10^{-6}$ m to $10^{-3}$ m, $\rho \sim 10^3$ kg/m$^3$, $\sigma_0 \sim 10^{-3}$ N/m to $10^{-1}$ N/m, $\gamma \sim 10^{-5}$ N/(m K) to $10^{-3}$ N/(m K), $k_{th} \sim 10^{-6}$ J/(m s K) to $10^{-3}$ J/(m s K), $q \sim 0$ J/(m$^2$ s K) to $10^2$ J/(m$^2$ s K), $\alpha \sim 10^{-7}$ m$^2$/s to $10^{-5}$ m$^2$/s, $\mu_0 \sim 10^{-3}$ Pa s to $10^2$ Pa s, $\lambda_1 \sim 10^{-7}$ s to $10^{-1}$ s, and $\lambda_2 \sim 10^{-7}$ s to $10^{-3}$ s. Thus, the typical values of the dimensionless numbers are $Bi \sim O(10^{-3}$–$10)$, $Bo \sim O(10^{-3}$–$10^{-1})$, $Ca \sim O(10^{-4}$–$10^{-1})$, $W \sim O(10^{-3}$–$10^{2})$, $\beta \sim O(10^{-3}$–$10^{-1})$, and $Pr \sim O(1$–$10^3)$. This parametric range will be used here to study the various modes of instability.

### A. Modes of instability

A viscoelastic liquid layer subjected to a purely VTG exhibits a stationary mode and two elastic instability modes.[23,27] The stationary mode is a consequence of the viscosity alone since it exists even for a Newtonian fluid. However, the two elastic oscillatory modes exist only in the case of a layer of an elastic liquid, and their emergence is a consequence of fluid elasticity. The elastic modes in the presence of the VTG possess the same growth rate and phase speed but travel in the opposite directions, i.e., one of the modes travels downstream ($s_i < 0$), whereas the other one travels upstream ($s_i > 0$). These elastic modes are presented in Fig. 1(a) with two blue circles representing the case of $\eta = 0$. However, the imposed HTG breaks the left-right symmetry and stabilizes the downstream mode with an increase in $\eta$. For the sake of brevity, henceforth, the upstream and downstream elastic modes arising due to the VTG will be simply referred to as the "upstream elastic mode" and "downstream elastic mode," respectively.

Patne *et al.*[37] demonstrated a stabilizing effect of the HTG on the long-wave instability mode in the case of a layer of a Newtonian liquid. A similar stabilizing effect also exists in the case of elastic modes, as presented in Fig. 1. The downstream elastic mode is suppressed at much lower $\eta$ than the upstream elastic mode. Interestingly, for low $\eta$, as shown in Fig. 1(a), the upstream elastic mode exhibits an increasing growth rate with an increase in the strength of the imposed HTG, $\eta$, i.e., becomes more unstable. However, Fig. 1(b) demonstrates that a further increase in $\eta$ by two orders of magnitude also leads to the stabilization of the upstream mode. Furthermore, when the upstream mode becomes stable, i.e., when $s_r < 0$, the mode also becomes downstream.

The stabilization of the elastic modes can be explained by the following argument: the emergence of the symmetric elastic modes is caused by the imposed VTG since they exist with $\eta = 0$. The imposed HTG induces a VTG, which then counteracts the imposed VTG. The term $\frac{\eta^2 Ma}{2(1+Bi)}\left(1 + \frac{Bi}{3}\right)$ in the base-state temperature equation (9b) represents the induced VTG. The *induced* VTG is of opposite sign and thus opposes the *imposed* VTG, thereby weakening the driving force for the elastic mode instability. This leads to the stabilization of the elastic modes shown in Fig. 1. When the *imposed* VTG and *induced* VTG are of the same magnitude, then the quantity $\frac{\eta^2 Ma}{2(1+Bi)}\left(1 + \frac{Bi}{3}\right) - 1$ must vanish, which after solving for $Ma$ at $Bi = 0$ yields $Ma = 2/\eta^2$ below which instabilities induced by the VTG can exist.

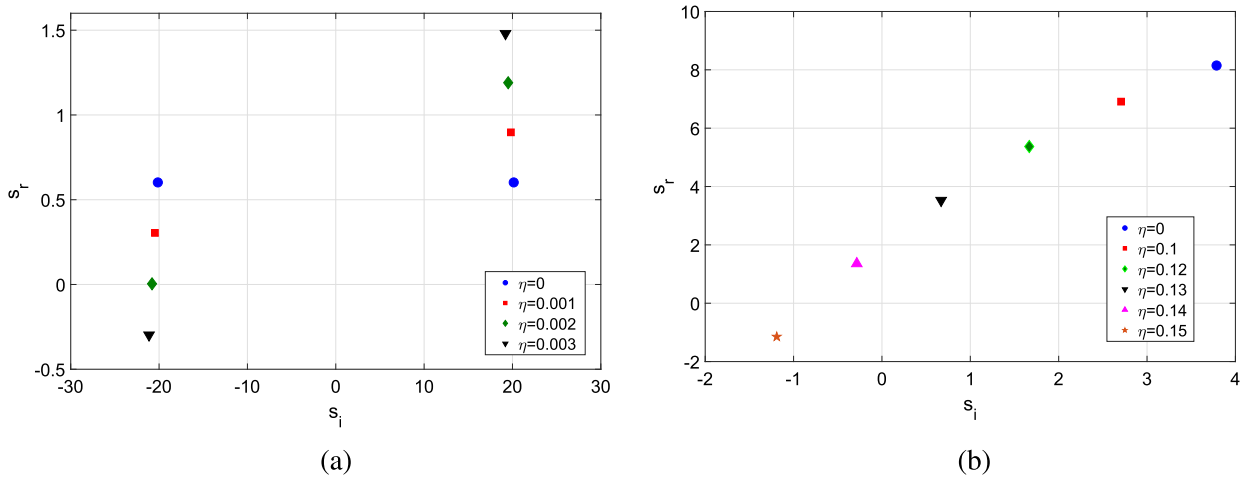


**FIG. 1.** Variation in the elastic modes with an increase in the strength of the HTG $\eta$ for the parameter set $Bi = 0$, $Bo = 0.1$, $Pr = 7$, $W = 0.1$, $Ma = 95$, $k = 4.5$, and $\beta = 0.01$ presented in the $s_r$–$s_i$ plane: (a) the case of low values of $\eta$. An imposed HTG causes the stabilization of the downstream ($s_i < 0$) elastic mode and the destabilization of the upstream ($s_i > 0$) elastic mode with an increase in $\eta$. (b) The case of higher values of $\eta$. Even the upstream elastic mode becomes stable at sufficiently high $\eta$. Note the switching of the propagation direction from upstream to downstream as the mode becomes stable. Recall that $s_r > 0$ implies an unstable mode.

With higher values of $W$, however, the imposed HTG fails to stabilize the upstream elastic mode, as illustrated in Fig. 2(b). This feature may arise from the destabilization caused by the HTG itself. Thus, even though the *induced* VTG nullifies the *imposed* VTG, thereby causing stabilization, the thermocapillary flow caused by the imposed HTG leads to the predicted destabilization. This also indicates that the driving mechanism for the upstream elastic mode for $\eta < 1$ is the *imposed* VTG, whereas for $\eta > 1$, it is the *imposed* HTG. Note an increase in $s_i$ of the upstream elastic mode with $\eta$ in Fig. 2(b) which implies that the HTG also fails to convert the upstream elastic mode to a downstream mode, unlike in the case of $W = 0.1$ shown in Fig. 1(b). Even though an HTG fails to stabilize the upstream elastic mode with an increase in $\eta$, the HTG still stabilizes the downstream elastic mode, see Fig. 2(a), albeit at a higher strength of an HTG than the case of $W = 0.1$ displayed in Fig. 1(a).

For the layer of a Newtonian liquid subjected to an OTG, Patne *et al.*[37] predicted the emergence of a new mode of instability originating as a consequence of the interaction between the imposed HTG and VTG, which will be referred to as the "Newtonian interaction mode" in the following discussion. This Newtonian interaction mode represents the dominant mode of instability at higher values of $\eta$, i.e., $\eta > 1$. Figures 3(a) and 4(a) show the stabilizing

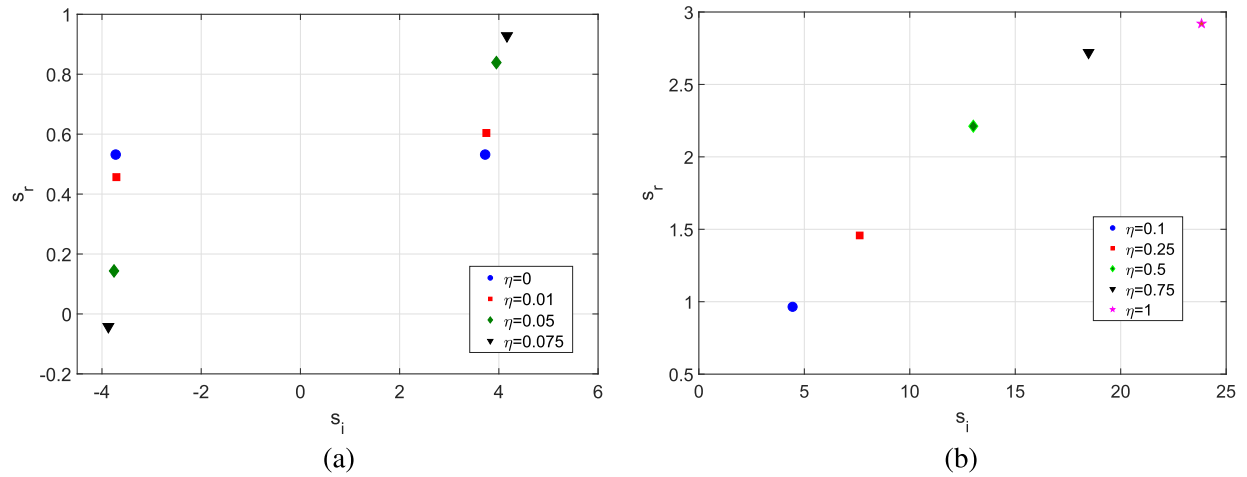


**FIG. 2.** Stabilizing/destabilizing impact of the HTG on the elastic modes with an increase in the strength of the HTG $\eta$ presented in the $s_r$–$s_i$ plane for $Bi = 0$, $Bo = 0.1$, $Pr = 7$, $W = 10$, $Ma = 1$, $k = 2.5$, and $\beta = 0.01$: (a) the case of smaller $\eta$. The stabilization of the downstream elastic mode due to the imposed HTG is evident, whereas the upstream elastic mode is destabilized. (b) The case of larger $\eta$. Due to higher values of $W$, the imposed HTG fails to stabilize the upstream elastic mode.

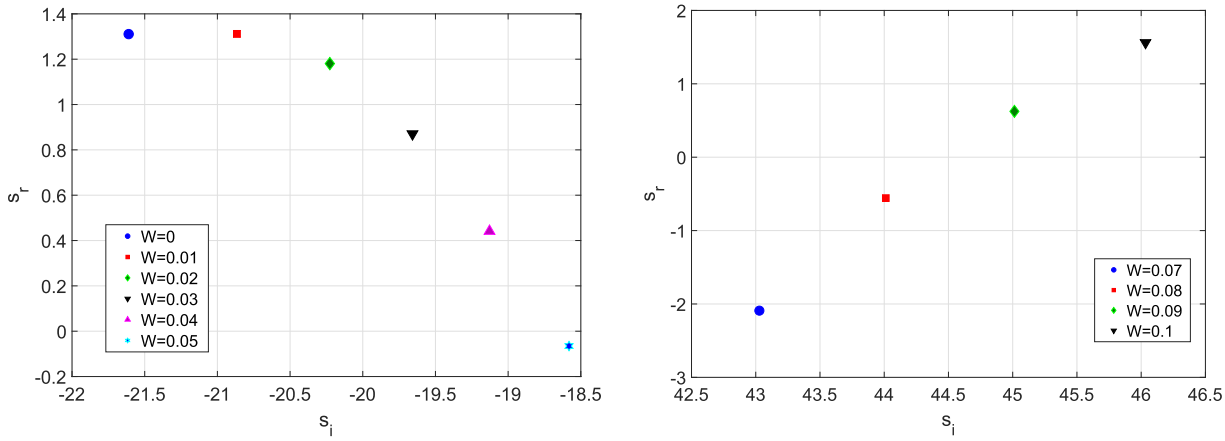


**FIG. 3.** Effect of fluid elasticity on the Newtonian interaction mode by Patne *et al.*[37] and the emergence of the new elastic unstable mode for $Bi = 0, Bo = 0.1, Pr = 7, \eta = 1$, and $\beta = 0.01$ presented in the $s_r$–$s_i$ plane: (a) variation in the growth rate of the Newtonian interaction mode with $W$ at $Ma = 35$ and $k = 0.3$. The stabilization of the Newtonian interaction mode by fluid elasticity at $W \approx 0.048$. (b) The new elastic mode arises as a consequence of the interaction between the elastic stresses and the viscous stresses enhanced by the thermocapillary flow driven by the imposed OTG at $Ma = 20$ and $k = 1.3$ for $W \approx 0.083$.

effect of an increasing Weissenberg number (relaxation constant) $W$ on the Newtonian interaction mode for $\eta = 1$ and $\eta = 10$, respectively. Interestingly, for a higher value of $\eta$, $\eta = 10$, the interaction mode initially exhibits an increase in the growth rate with $W$. A further increase in $W$ thereafter causes a stabilizing effect, as shown in Fig. 4(a). Thus, the elastic stresses represented by $W$ have a strong stabilizing effect on the Newtonian interaction mode. In the case of the Oldroyd-B liquid, the Newtonian interaction mode at high $\eta$, however, is replaced by a new instability mode arising from the interaction between the HTG, the *imposed* VTG, and the elastic stresses. Henceforth, the new instability mode will be referred to as the "new elastic mode." The destabilization of such a mode due to an increase in $W$ is shown in Figs. 3(b) and 4(b). Since for the destabilization of the new elastic mode the value of $W$ should exceed a certain threshold, this mode does not exist in layers of a Newtonian liquid that were the subject of the analysis by Patne *et al.*[37] Note also that the Newtonian interaction mode is a downstream traveling mode, whereas the new elastic mode is an upstream traveling one.

To understand the origin of the new elastic mode, the spatial variation of the perturbations for the streamwise velocity and temperature at the instability threshold are presented in Fig. 5. In the

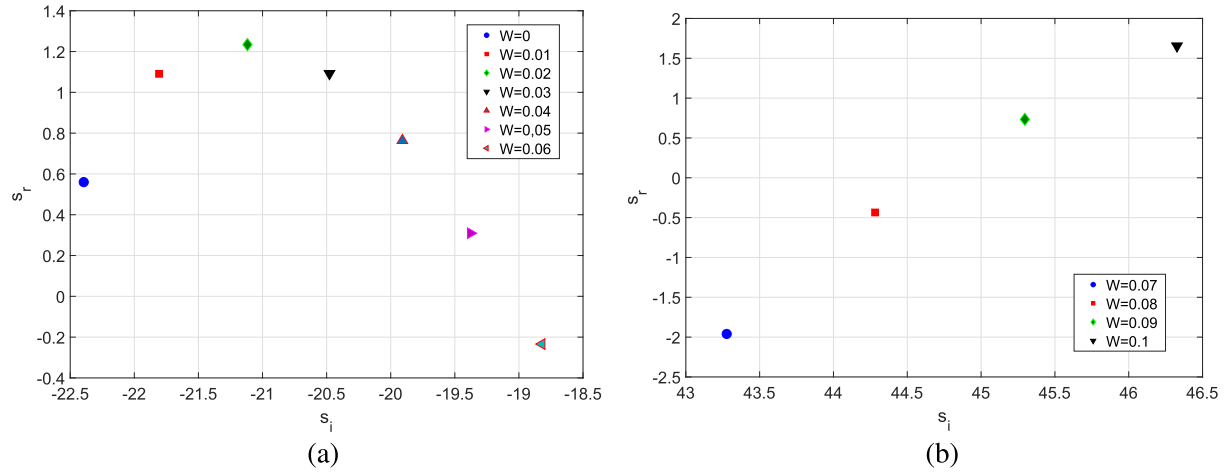


**FIG. 4.** Effect of fluid elasticity on the Newtonian interaction mode and the emergence of the new elastic unstable mode for $Bi = 0, Bo = 0.1, Pr = 7, \eta = 10$, and $\beta = 0.01$: (a) variation in the growth rate of the Newtonian interaction mode with $W$ at $Ma = 3.5$ and $k = 0.3$. (b) The emergence of a new elastic mode arises as a consequence of the interaction between the elastic stresses and the viscous stresses enhanced by the thermocapillary flow driven by the imposed OTG at $Ma = 2$ and $k = 1.3$.

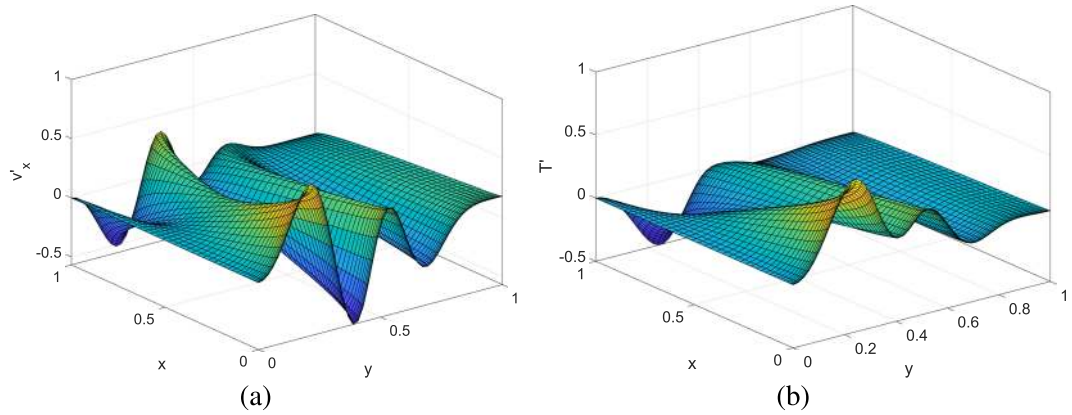


**FIG. 5.** Normalized perturbation fields for the new elastic mode in the case of the parameter set of $Bi = 0, Bo = 0.1, Pr = 7, \eta = 1, Ma = 16.41, k = 1.31, W = 0.1, \beta = 0.01$, and $Ca = 0.01$ for the marginally stable eigenvalue $s = 43.580\,37i$: (a) $v_x' = \Re[\widetilde{v}_x \exp(ikx)]$ and (b) $T' = \Re[\widetilde{T}\exp(ikx)]$. The length of the domain in the $x$-direction is the wavelength of the perturbations $2\pi/k$. For convenience, both axes are normalized to the interval $[0, 1]$. The perturbations exhibit the strongest variation near the substrate instead of the free surface where the Marangoni stresses are active. This implies that the thermocapillary flow induced by the imposed HTG plays the major role in causing the new elastic mode via the shear stress at the substrate. Note that the corresponding field for $v_y' = \Re[\widetilde{v}_y \exp(ikx)]$ looks very similar to that for $T'$.

case of instabilities introduced due to thermocapillarity, the perturbations typically exhibit the strongest variation at or near the free surface since the thermocapillary stresses act there and drive the emerging flow.[27] However, the perturbations corresponding to the new elastic mode exhibit their strongest variation near the substrate instead, i.e., at $y = 0$. This implies that the Marangoni stresses in the perturbed state might not play a major role in introducing the new elastic mode, which is indeed the case as illustrated in Table I.

In Table I, we present the eigenvalues obtained in the presence/absence of the Marangoni term in the tangential stress balance at the free surface for the perturbed state, Eq. (14c). The two columns on the right show that the Marangoni stresses in the perturbed state at the free surface $y = 1$ have a stabilizing effect on the new elastic mode. Note that the Marangoni term in the base-state tangential stress balance equation (8b) has been retained for both the cases, so the base state remains unchanged, and the thermocapillary flow is present due to the imposed HTG. The thermocapillary base-state flow induced by the imposed HTG is necessary for the emergence of the new elastic mode since the latter is absent in a viscoelastic liquid layer subjected to a purely VTG.[23,27] We conclude that the base-state thermocapillary flow introduces the new elastic mode via the disturbances in the bulk and the thermocapillary stresses acting at the free surface stabilize the new elastic mode.

## B. Critical parameters

The variation in the growth rate of the new elastic mode with the disturbance wavenumber for a specified parameter set is presented in Fig. 6(a). Note that the curves display the growth rate of the most unstable (least stable) mode at a given $k$, which results in multiple local maxima. The unstable peaks in the curves of Fig. 6(a) in $k \in [0.5, 2]$ correspond to the new elastic mode. For $k < 0.5$ and $k > 2$, the extension of the long-wave mode to higher $k$ exhibits a higher growth rate than the new elastic mode. This results in the emergence of the curves that display sharp corners, as shown in Fig. 6(a). Thus, the stretch of the growth rate curve in the domain $k \in [0.5, 2]$ is due to the new elastic mode whereas those in the domains $k < 0.5$ and $k > 2$ are due to the extension of the long-wave mode to higher $k$. A combination of these leads to the multiple peaks in the growth rate curves. As seen in Fig. 6(a), the growth rate of the new elastic mode and the wavenumber of the fastest growing mode increase with the Marangoni number $Ma$.

**TABLE I.** The leading eigenvalues corresponding to the new elastic mode in the presence and absence of the Marangoni term $\left[-i\,k\,Ma\left(\widetilde{T} + \partial_y \bar{T}\,\widetilde{\xi}\right)\right]$ in the tangential stress balance at the free surface equation (14c) shown in the middle and right columns, respectively, for $\beta = 0.01$ and $Ca = 0.01$. Note that $s_r > 0$ implies an unstable mode.

| Parameters | With $Ma$ term in Eq. (14c) | Without $Ma$ term in Eq. (14c) |
|---|---|---|
| $W = 0.1, k = 1.3, Ma = 15, \eta = 1$ | $-0.587\,544 + 42.319\,8i$ | $0.172\,870 + 43.197\,7i$ |
| $W = 0.1, k = 1.3, Ma = 20, \eta = 1$ | $1.559\,90 + 46.033\,92i$ | $2.358\,46 + 47.129\,2i$ |
| $W = 0.1, k = 1, Ma = 20, \eta = 1$ | $0.669\,364 + 37.303\,4i$ | $1.684\,70 + 38.361\,4i$ |
| $W = 0.2, k = 1, Ma = 20, \eta = 1$ | $5.499\,76 + 45.342\,2i$ | $6.335\,89 + 46.759\,0i$ |
| $W = 0.2, k = 1, Ma = 20, \eta = 2$ | $10.817\,4 + 74.246\,7i$ | $11.298\,0 + 76.722\,6i$ |

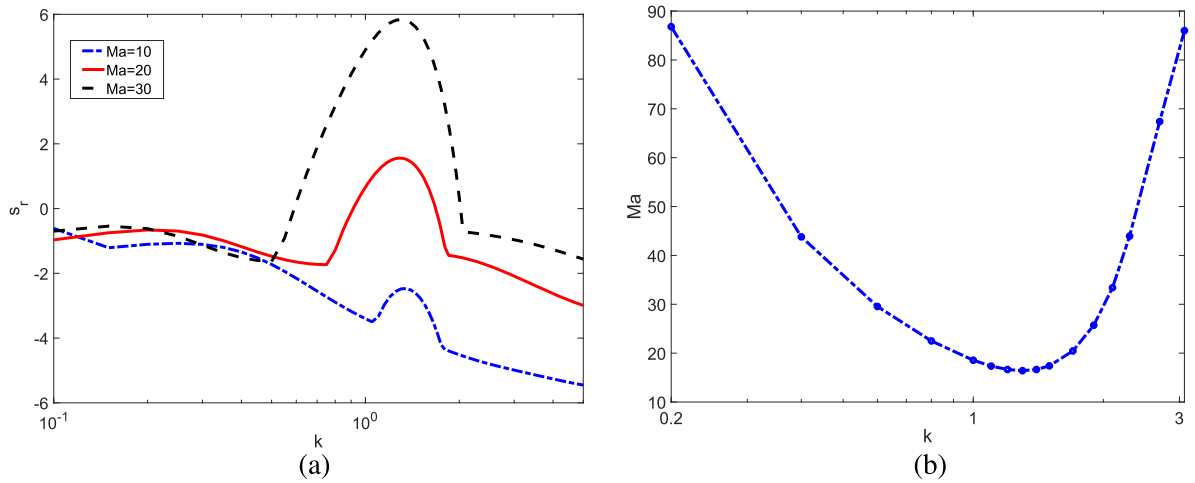


**FIG. 6.** Growth rate and neutral stability curve for the new elastic unstable mode at $Bi = 0, Bo = 0.1, Pr = 7, \eta = 1, Ca = 0.01, W = 0.1$, and $\beta = 0.01$: (a) variation in the growth rate with the wavenumber $k$ and (b) the neutral stability curve in the $Ma - k$ plane. The system is unstable in the domain above the neutral stability curve.

For a further analysis, evaluation of the critical parameters $k_c$ and $Ma_c$ is necessary. Figure 6(b) presents a neutral stability curve for the same parameter set. The critical wavenumber $k_c$ corresponds to the minimum of this curve, i.e., $k_c \sim 1.3$, and the critical Marangoni number $Ma_c$ corresponding to $k = k_c$ from Fig. 6(b) is $Ma_c \sim 16.4$. A similar procedure has been followed to determine $Ma_c$ in the following discussion.

The effect of variation in the elasticity on the critical Marangoni number of the Newtonian interaction mode, the new elastic mode, and the upstream elastic mode is displayed in Fig. 7. The upstream elastic mode was shown above to survive the stabilization caused by the imposed HTG in Fig. 2(b) provided that $W$ is sufficiently high. Such a condition is met for $W \sim 1$, and thus in Fig. 7, we show switching of the most unstable mode from the new elastic mode to the upstream elastic mode at $W \sim 1$. In addition, the Newtonian interaction mode is found to be stable for $W > 0.075$. Note that as shown in Fig. 7, the neutral curves for the Newtonian interaction mode reach an asymptote at a certain value of $W$ denoted as $W = W_N$.

It must be noted that the value of $W = W_N$ at which the Newtonian interaction mode loses its dominance depends very weakly on $\eta$. It also depends on other parameters of the problem. We have

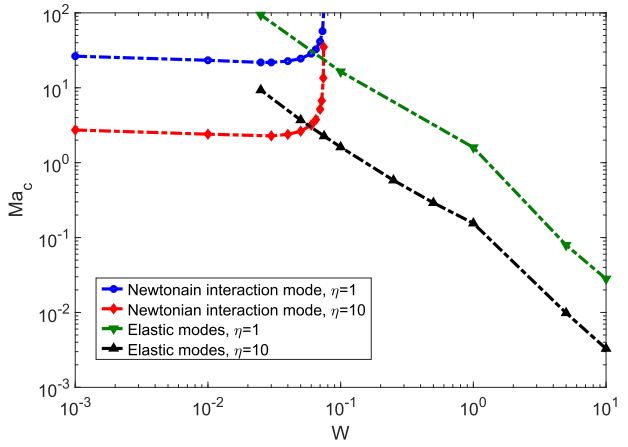


**FIG. 7.** Variation in the critical Marangoni number $Ma_c$ with $W$ for the parameter set $Bi = 0, Bo = 0.1, Ca = 0.01, \beta = 0.01$, and $Pr = 7$. In the legend, the term "elastic modes" refers to the new elastic mode and the upstream elastic mode together. The new elastic and the upstream elastic modes are the dominant modes of instability in the domains $0.075 < W < 1$ and $W > 1$, respectively, and the discontinuity in the slope of the corresponding curves at $W = 1$ is a consequence of this mode switching. The Newtonian interaction mode prevalent for $W < 0.075$ is stabilized by the elastic stresses for $W > 0.075$. The new elastic and the upstream elastic modes show a characteristic scaling as $Ma_c \sim W^{-1}$ and $Ma_c \sim W^{-1.5}$, respectively. The base-state is linearly stable for $Ma < Ma_c$.

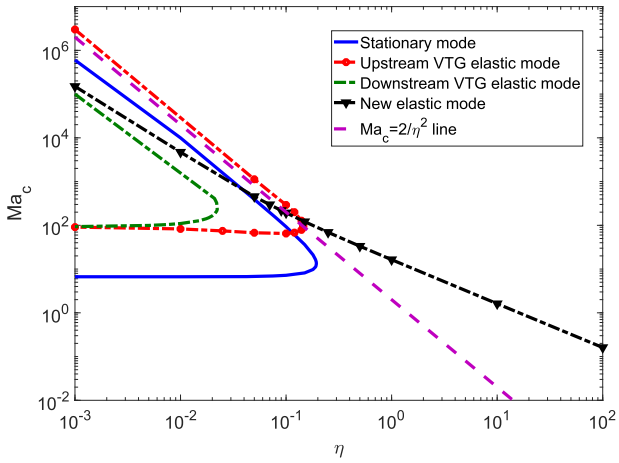


**FIG. 8.** Variation in $Ma_c$ with $\eta$ at $Bi = 0, Bo = 0.1, Ca = 0.01, W = 0.1, \beta = 0.01$, and $Pr = 7$. Since $W < 1$, the stationary and elastic modes introduced by the imposed VTG are stabilized by the imposed HTG. The new elastic mode exhibits a characteristic scaling as $Ma_c \sim \eta^{-1}$ for $\eta > 0.2$. For the entire range of $\eta$, it exhibits the scaling $Ma_c \sim 1/\eta^n$, where the exponent $n$ varies from 2 at very low $\eta$ to 1 at high $\eta$.

found that a decrease in $Ca$ by one order from $Ca = 0.01$ to $Ca = 0.001$ causes $W_N$ to weakly reduce from 0.075 to 0.071, while other parameters are kept the same as in Fig. 7. Similarly, with an increase in the Prandtl number from $Pr = 7$ to $Pr = 50$, $W_N$ reduces significantly from 0.075 to 0.0146, almost at the same inverse proportion as the change in $Pr$. Thus, a variation in $Ca$ weakly affects $W_N$; however, the effect of a variation in $Pr$ on $W_N$ is strong. We have also found that the variation in the Biot number $Bi$ and the Bond number $Bo$ does not affect $W_N$ significantly.

In Fig. 7, the variation in the critical Marangoni number with $W$ is presented for two selected values of $\eta$. To obtain a complete picture of the instability onset as the strength of the HTG $\eta$ varies, the different stability modes are tracked, and the results are presented in Fig. 8. It is shown that for sufficiently small values of $\eta$, the instability is long-wave stationary. For sufficiently large values of $\eta$, the new elastic mode of instability, which is oscillatory by nature, takes over. Since the downstream elastic mode is stabilized at a much lower strength of the HTG than the upstream elastic mode seen in Fig. 1, the island of unstable values of $Ma_c$ is smaller for the downstream elastic mode than the one for the upstream elastic mode. Interestingly, the upper boundary of the island for the upstream elastic mode extends beyond the asymptotic line $Ma_c = 2/\eta^2$. This crossing is possible because of the acting elastic stresses at play. Thus, to destabilize the base-state flow, the *induced* VTG not only has to counteract the *imposed* VTG but it has to also overcome the elastic stresses responsible for the stabilization of the elastic modes. This feature enables the neutral curve of the VTG mode to cross the asymptotic boundary unlike that of the stationary mode remaining always underneath it. The critical wavenumber $k_c$ shows a small variation with $\eta$ for all these modes. Thus, $k_c \sim 4.4$, $k_c \sim 4.6$, and $k_c \sim 1.3$ for the upstream elastic, downstream elastic, and new elastic modes, respectively, whereas the stationary mode is long-wave with $k_c = 0$. It must be also noted that the stationary mode is *negligibly* affected by the elasticity of the fluid.

We deduce from Figs. 7 and 8 that the critical Marangoni number for the new elastic mode shows scaling as $Ma_c \sim W^{-1}$ and $Ma_c \sim \eta^{-1}$. Combining both scalings yields $Ma_c \sim (\eta W)^{-1}$. The degree of elasticity of a viscoelastic fluid is represented by the parameter $\omega$ defined as the ratio between the first normal stress difference and the tangential stress.[41] Accounting for the base state given by Eq. (9a), $\omega$ becomes

$$\omega = \frac{\bar{\tau}_{xx} - \bar{\tau}_{yy}}{\bar{\tau}_{xy}} = (W - \beta)\eta Ma. \tag{18}$$

However, since $W \gg \beta$,[41] $\omega \approx W\eta Ma$. For a Newtonian liquid undergoing a rectilinear flow, $\bar{\tau}_{xx} - \bar{\tau}_{yy} = 0$; thus, $\omega = 0$. The numerator of $\omega$ describes the elastic stresses, whereas the denominator is related to the viscous stresses. If the elastic and viscous stresses are comparable, then $\omega = O(1)$, thereby yielding $Ma \sim (\eta W)^{-1}$, which is indeed the scaling exhibited by the new elastic mode. Thus, the new elastic mode becomes unstable when the viscous and elastic stresses induced by the thermocapillary flow are comparable in their magnitude. This also shows the important role played by the elastic stresses in destabilizing the new elastic mode.

To further understand the new elastic mode, the capillary number $Ca$ and Prandtl number $Pr$ are varied while the rest of the parameters remain constant, and the resulting change in the onset of the new elastic mode is then reflected through the variation in $Ma_c$, as presented in Fig. 9. An increase in $Pr$ leads to the stabilization, as shown in Fig. 9(b).

The effect of variation in the other parameters, $Bi$ and $Bo$, on the critical parameters for the new elastic mode is found to be negligible. Figure 10 demonstrates the effect of variation in the retardation parameter $\beta$, which is related to the solvent concentration in polymer solutions. A decrease in $\beta$ corresponds to a reduction in the solvent concentration, leading to an enhancement in the liquid elasticity. This enhancement results in a decrease in $Ma_c$ pointing to the destabilization, as presented in Fig. 10.

For sufficiently high values of $W$, e.g., $W > 1$, the induced VTG fails to stabilize the upstream elastic mode, as demonstrated in Fig. 2(b). Thus, for $W > 1$, the stability regimes shown in Fig. 8 alter

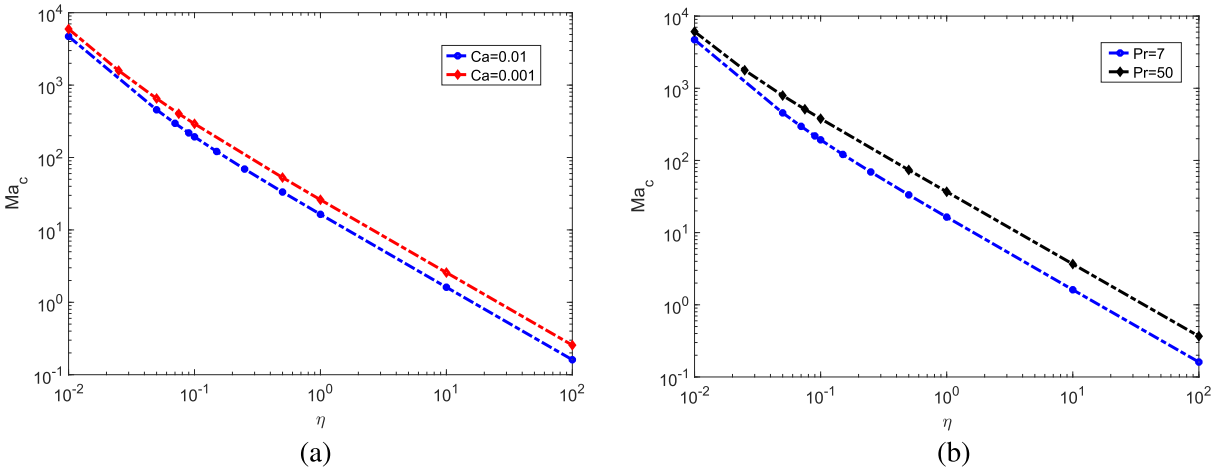


**FIG. 9.** Effect of variation in $Ca$ and $Pr$ on the new elastic unstable mode presented in the $Ma_c - \eta$ plane for $Bi = 0$, $Bo = 0.1$, $W = 0.1$, and $\beta = 0.01$: (a) the destabilization of the new elastic mode with an increase in $Ca$ and (b) the stabilization caused by an increase in $Pr$.

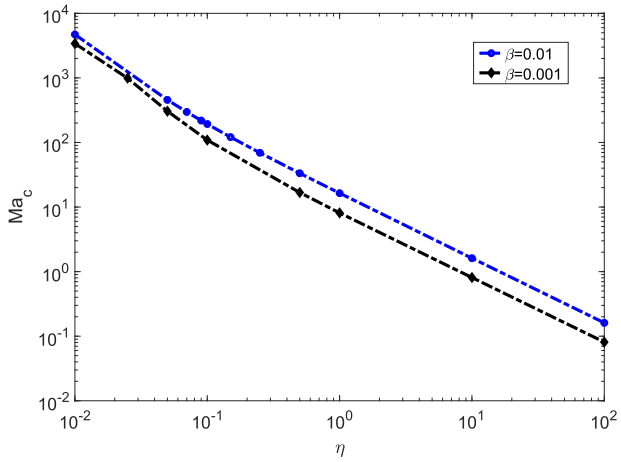


**FIG. 10.** Variation in $Ma_c$ with $\eta$ at $Bi = 0$, $Bo = 0.1$, $Ca = 0.01$, $W = 0.1$, and $Pr = 7$ for two values of the retardation parameter $\beta$. A decrease in the retardation parameter results in a destabilizing effect on the new elastic mode.

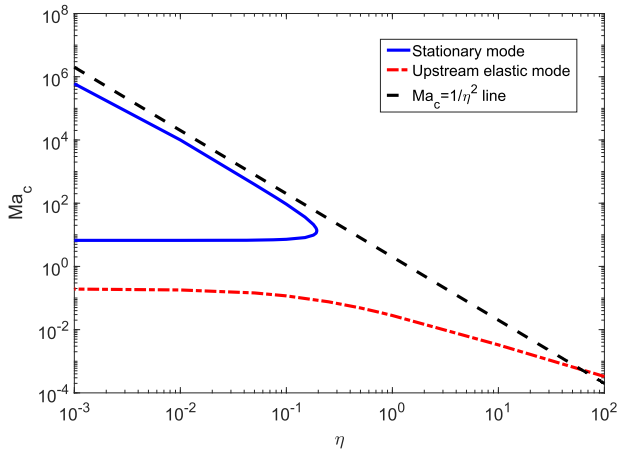


**FIG. 11.** Variation in $Ma_c$ with $\eta$ at $Bi = 0$, $Bo = 0.1$, $Ca = 0.01$, $W = 10$, and $Pr = 7$ for $W = 1$ compared with Fig. 8. Due to a sufficiently high value of $W$, the imposed HTG fails to stabilize the upstream elastic mode, thereby making it the dominant mode of instability for any value of $\eta$. For $\eta > 0.5$, the upstream elastic mode shows scaling $Ma_c \sim \eta^{-1}$, which is the same as the new elastic mode. Since the fluid elasticity negligibly affects the stationary VTG mode, it is stabilized by the HTG via the *presence of the induced* VTG.

significantly. Figure 11 depicts the altered picture for $W = 10$, for which the upstream elastic mode represents the dominant mode of instability for any value of $\eta$. For $\eta > 0.5$, the upstream elastic mode exhibits scaling $Ma_c \sim \eta^{-1}$, which is the same as for the new elastic mode. Note that in this case, the critical wavenumber $k_c \approx 2.4$ with a small variation over the entire range of $\eta$.

## V. SUMMARY

The present work focuses on the linear stability analysis of a viscoelastic liquid layer with a free deformable interface exposed to the ambient gas lying on a planar solid wall and subjected to an oblique temperature gradient (OTG) with the horizontal and vertical components, HTG and VTG, respectively. The dynamics of the liquid is described by employing the Oldroyd-B model. Linear stability analysis reveals that if subjected to a purely VTG, a viscoelastic liquid layer exhibits a long-wave viscous stationary mode and two elastic oscillatory modes with the same growth rate and phase speeds of opposite signs. These oscillatory modes correspond to the disturbances propagating in the opposite directions and are referred to as the upstream and downstream elastic modes. Both of these modes are stabilized with an increase in the magnitude of the imposed HTG, i.e., $\eta$ at low values of the Weissenberg number $W$. This stabilization originates from the additional VTG *induced* by the presence of the *imposed* HTG in the base-state flow. The induced VTG counteracts the imposed one, thereby nullifying the mechanism driving the emergence of the elastic modes. At high Weissenberg numbers $W$, however, the imposed HTG stabilizes the downstream elastic mode, but the upstream elastic mode remains unstable.

At a certain value of $W = W_N$, the Newtonian interaction mode is stabilized by the elastic stresses in the liquid, being only negligibly affected by them for $W < W_N$. In addition, in the parameter ranges considered here, the elastic modes are stabilized by the HTG for $W < W_N$. Thus, for $W < W_N$, the stability properties of the liquid layer are the same as those of a Newtonian liquid layer studied by Patne *et al.*,[27] where the interaction mode emerging from the induction of an extra VTG sets in. However, for $W > W_N$, the Newtonian interaction instability mode is stabilized by the fluid elasticity and is replaced by a new elastic mode that becomes the dominant mode of instability for $W_N < W < 1$, while for $W > 1$, the upstream elastic instability mode dominates for any value of $\eta$. It is emphasized that the value $W = W_N$ depends weakly on $\eta$ and the capillary number $Ca$, and strongly on the Prandtl number $Pr$.

The new elastic mode, which does not exist in a layer of a Newtonian liquid, results from the presence of the thermocapillary flow generated by the imposed HTG and the perturbations triggering this mode, which are confined near the wall. In addition, a stress balance reveals that for destabilization of the new elastic mode, the viscous shear and the elastic stresses must be comparable, which explains the scaling exhibited by the new elastic mode as $Ma_c \sim (\eta W)^{-1}$. A further analysis reveals a stabilizing effect of an increase in $Pr$, a decrease in $Ca$, and an increase in the retardation number $\beta$.

Since the critical wavenumber of the instability modes predicted here varies widely, the present work illustrates a potential application of the imposed OTG and the ensuing thermocapillary instability in a viscoelastic liquid layer in achieving the desired pattern relevant in industrial processes and experimental settings.

## ACKNOWLEDGMENTS

This research was supported by Grant No. 356/18 from the Israel Science Foundation (ISF). R.P. was partially supported by the Technion Funds Postdoctoral Fellowship. Y.A. was partially supported by the Millstone/St. Louis Chair in Civil and Environmental Engineering. A.O. was partially supported by the David T. Siegel Chair in Fluid Mechanics.

## DATA AVAILABILITY

The data that support the findings of this study are available within the article.

## REFERENCES


[1]K. N. Kowal, S. H. Davis, and P. W. Voorhees, "Thermocapillary instabilities in a horizontal liquid layer under partial basal slip," J. Fluid Mech. **855**, 839–859 (2018).

[2]M. Lappa, *Thermal Convection: Patterns, Evolution and Stability* (Wiley, 2010).

[3]S. F. Kistler and P. M. Schweizer, *Liquid Film Coating: Scientific Principles and Their Technological Implications* (Springer, Dordrecht, 1997).

[4]A. Karbalaei, R. Kumar, and H. J. Cho, "Thermocapillarity in microfluidics—A review," Micromachines **7**, 13 (2016).

[5]J. P. Singer, "Thermocapillary approaches to the deliberate patterning of polymers," J. Polym. Sci., Part B: Polym. Phys. **55**, 319–352 (2017).

[6]R. Mukherjee and A. Sharma, "Instability, self-organization and pattern formation in thin soft films," Soft Matter **11**, 8717–8740 (2015).

[7]J. R. A. Pearson, "On convection cells induced by surface tension," J. Fluid Mech. **4**, 489–500 (1958).

[8]H. Bénard, "Les tourbillons cellulaires dans une nappe liquide transportant de la chaleur par convection en régime permanent," Annu. Chem. Phys. **23**, 62–144 (1901).

[9]L. E. Scriven and C. V. Sternling, "On cellular convection driven by surface-tension gradients: Effects of mean surface tension and surface viscosity," J. Fluid Mech. **19**, 321–340 (1964).

[10]K. A. Smith, "On convective instability induced by surface-tension gradients," J. Fluid Mech. **24**, 401–414 (1966).

[11]S. H. Davis and G. M. Homsy, "Energy stability theory for free-surface problems: Buoyancy-thermocapillary layers," J. Fluid Mech. **98**, 527–553 (1980).

[12]C. Pérez-Garcia and G. Carneiro, "Linear stability analysis of Bénard-Marangoni convection in fluids with a deformable free surface," Phys. Fluids A **3**, 292–298 (1991).

[13]S. H. Davis, "Thermocapillary instabilities," Annu. Rev. Fluid Mech. **19**, 403–435 (1987).

[14]M. K. Smith and S. H. Davis, "Instabilities of dynamic thermocapillary liquid layers. Part 1. Convective instabilities," J. Fluid Mech. **132**, 119–144 (1983).

[15]M. K. Smith and S. H. Davis, "Instabilities of dynamic thermocapillary liquid layers. Part 2. Surface-wave instabilities," J. Fluid Mech. **132**, 145–162 (1983).

[16]D. Schwabe, U. Möller, J. Schneider, and A. Scharmann, "Instabilities of shallow dynamic thermocapillary liquid layers," Phys. Fluids A **4**, 2368–2381 (1992).

[17]R. J. Riley and G. P. Neitzel, "Instability of thermocapillary-buoyancy convection in shallow layers. Part 1. Characterization of steady and oscillatory instabilities," J. Fluid Mech. **359**, 143–164 (1998).

[18]S. Benz, P. Hintz, R. J. Riley, and G. P. Neitzel, "Instability of thermocapillary-buoyancy convection in shallow layers. Part 2. Suppression of hydrothermal waves," J. Fluid Mech. **359**, 165–180 (1998).

[19]M. F. Schatz and G. P. Neitzel, "Experiments on thermocapillary instabilities," Annu. Rev. Fluid Mech. **33**, 93–127 (2001).

[20]N. A. Ospennikov and D. Schwabe, "Thermocapillary flow without return flow-linear flow," Exp. Fluids **36**, 938–945 (2004).

[21]D. Schwabe, "Convective instabilities in complex systems with partly free surface," J. Phys.: Conf. Ser. **64**, 012001 (2007).

[22]D. Getachew and S. Rosenblat, "Thermocapillary instability of a viscoelastic liquid layer," Acta Mech. **55**, 137–149 (1985).

[23]G. Lebon, P. Parmentier, O. Teller, and P. C. Dauby, "Bénard-Marangoni instability in a viscoelastic Jeffreys' fluid layer," Rheol. Acta **33**, 257–266 (1994).

[24]G. Lebon and A. Cloot, "An extended thermodynamic approach to non-Newtonian fluids and related results in Marangoni instability problem," J. Non-Newtonian Fluid Mech. **28**, 61–76 (1988).

[25]P. C. Dauby, P. Parmentier, G. Lebon, and M. Grmela, "Coupled buoyancy and thermocapillary convection in a viscoelastic Maxwell fluid," J. Phys.: Condens. Matter **5**, 4343–4352 (1993).

[26]P. G. Siddheshwar, G. N. Sekhar, and G. Jayalatha, "Surface tension driven convection in viscoelastic liquids with thermorheological effect," Int. Commun. Heat Mass Transfer **38**, 468–473 (2011).

[27]R. Patne, Y. Agnon, and A. Oron, "Marangoni instability in the linear Jeffreys fluid with a deformable surface," Phys. Rev. Fluids **5**, 084005 (2020).

[28]M. Li, S. Xu, and E. Kumacheva, "Convection in polymeric fluids subjected to vertical temperature gradients," Macromolecules **33**, 4972–4978 (2000).

[29]K.-X. Hu, M. He, and Q.-S. Chen, "Instability of thermocapillary liquid layers for Oldroyd-B fluid," Phys. Fluids **28**, 033105 (2016).

[30]K.-X. Hu, M. He, Q.-S. Chen, and R. Liu, "Linear stability of thermocapillary liquid layers of a shear-thinning fluid," Phys. Fluids **29**, 073101 (2017).

[31]K.-X. Hu, C.-Y. Yan, and Q.-S. Chen, "Instability of thermocapillary-buoyancy convection in droplet migration," Phys. Fluids **31**, 122101 (2019).

[32]A. A. Nepomnyashchy, I. B. Simanovskii, and L. M. Braverman, "Stability of thermocapillary flows with inclined temperature gradient," J. Fluid Mech. **442**, 141–155 (2001).

[33]O. E. Shklyaev and A. A. Nepomnyashchy, "Thermocapillary flows under an inclined temperature gradient," J. Fluid Mech. **504**, 99–132 (2004).

[34]A. A. Nepomnyashchy and I. B. Simanovskii, "Marangoni instability in ultrathin two-layer films," Phys. Fluids **19**, 122103 (2007).

[35]A. A. Nepomnyashchy and I. B. Simanovskii, "Dynamics of ultra-thin two-layer films under the action of inclined temperature gradients," J. Fluid Mech. **631**, 165–197 (2009).

[36]A. A. Nepomnyashchy and I. B. Simanovskii, "Marangoni waves in a two-layer film under the action of an inclined temperature gradient," Phys. Fluids **26**, 082102 (2014).

[37]R. Patne, Y. Agnon, and A. Oron, "Thermocapillary instabilities in a liquid layer subjected to an oblique temperature gradient," J. Fluid Mech. **906**, A12 (2021).

[38]I. B. Simanovskii, A. Viviani, F. Dubois, and J.-C. Legros, "The influence of the horizontal component of the temperature gradient on nonlinear convective oscillations in two-layer systems," Phys. Fluids **24**, 102108 (2012).

[39]A. I. Mizev and D. Schwabe, "Convective instabilities in liquid layers with free upper surface under the action of an inclined temperature gradient," Phys. Fluids **21**, 112102 (2009).

[40]R. G. Larson, *Constitutive Equations for Polymer Melts and Solutions* (Butterworths, Boston, 1988).

[41]R. B. Bird, R. C. Armstrong, and O. Hassager, *Dynamics of Polymeric Liquids*, Fluid Mechanics Vol. 1 (John Wiley, New York, 1977).

[42]J. G. Oldroyd, "On the formulation of rheological equations of state," Proc. R. Soc. London, Ser. A **200**(1063), 523–541 (1950).

[43]R. B. Bird, R. C. Armstrong, and O. Hassager, *Dynamics of Polymeric Liquids*, Kinetic Theory Vol. 2 (John Wiley, New York, 1977).

[44]T. C. B. McLeish and R. G. Larson, "Molecular constitutive equations for a class of branched polymers: The pom-pom polymer," J. Rheol. **42**, 81–110 (1998).

[45]A. E. Likhtman and R. S. Graham, "Simple constitutive equation for linear polymer melts derived from molecular theory: Rolie-Poly equation," J. Non-Newtonian Fluid Mech. **114**, 1–12 (2003).

[46]P. J. Schmid and D. S. Henningson, *Stability and Transition in Shear Flows* (Springer, New York, 2001).

[47]L. N. Trefethen, *Spectral Methods in MATLAB* (SIAM, Philadelphia, 2000).